# Contributions to Electrostatic Interactions on Protein Transport in Membrane Systems

**Douglas B. Burns and Andrew L. Zydney**
Dept. of Chemical Engineering, University of Delaware, Newark, DE 19716

*Several recent studies have demonstrated the importance of electrostatic interactions on the transport of charged proteins through porous membranes. The objective of this study is to compare predictions of available hydrodynamic and partitioning models with experimental data for the sieving coefficient of ovotransferrin through both positively and negatively charged membranes over a range of solution conditions. Model calculations were performed with all parameters evaluated from independent experimental measurements. The membrane pore-size distribution was determined from dextran sieving data, and the membrane surface charge was evaluated from streaming potential measurements. The model properly predicts the complex effects of solution pH and ionic strength on protein transmission in the presence of both attractive and repulsive electrical interactions. Model simulations were performed to highlight the key contributions to protein transport.*

## Introduction

Ultrafiltration has traditionally been viewed as a purely size-based separation process. However, there is extensive experimental evidence that protein transport through semipermeable membranes is also strongly affected by electrostatic interactions. For example, Pujar and Zydney (1994) showed that the transmission of bovine serum albumin (BSA) through a 100,000 molecular weight cut-off membrane decreased by nearly two orders of magnitude as the salt concentration was reduced from 150 to 1.5 mM. This large increase in protein rejection was attributed to the increased electrostatic exclusion of the charged BSA from the membrane pores at low ionic strength. Nakao et al. (1988), Balakrishnan and Agarwal (1996), and Burns and Zydney (1999) all evaluated the effect of solution pH on protein transmission, with the maximum transmission typically attained near the protein isoelectric point (that is, at the pH where the protein has no net electrical charge). Several studies (Miyama et al., 1988; Millesime et al., 1994; van Reis et al., 1999) have shown that protein transport is also a function of the membrane surface charge characteristics, with protein transmission being significantly reduced under conditions where the membrane and protein have like charge due to the increased electrostatic repulsion. These electrostatic interactions can be exploited to achieve very high resolution protein separations by membrane filtration (van Reis et al., 1999).

There have also been a number of theoretical analyses of the effects of electrostatic interactions on solute transport in membrane systems. Most of these studies have focused on evaluating the equilibrium partition coefficient for a charged solute in a narrow pore. Munch et al. (1979) presented a very simple model for electrostatic repulsion in which the protein radius was assumed to increase, and the pore radius decrease, by the thickness of the electrical double layer. Malone and Anderson (1978) and Causserand et al. (1996) developed more sophisticated analyses based on the electrostatic interactions between a charged hard sphere and two flat plates. The most complete analysis of electrostatic interactions in membrane systems was presented by Smith and Deen (1980, 1983) who evaluated the potential energy of interaction for a charged spherical solute in a charged cylindrical pore by solving the linearized Poisson-Boltzmann equation. Initial calculations (Smith and Deen, 1980) were presented for a sphere located at the pore axis (often called the centerline approximation). This work was subsequently extended to provide expressions for the energy of interaction as an explicit function of radial position (Smith and Deen, 1983). Pu-

Correspondence concerning this article should be addressed to A. L. Zydney.

jar and Zydney (1997) included the effects of charge regulation on the solute partition coefficient using the same basic theoretical formalism.

Although these analyses provide reasonable qualitative descriptions of the experimental results, quantitative comparisons between theory and data are limited. Malone and Anderson (1978) used their theoretical model to analyze experimental data for latex diffusion through track-etched membranes, but the results were limited to very small values of the solute to pore size ratio ($r_s/r_p < 0.15$). Mitchell and Deen (1986) found that BSA rejection through track-etched polycarbonate membranes was significantly greater than that predicted by the analysis of Smith and Deen (1983), which they attributed to protein adsorption within the membrane pores. Pujar and Zydney (1994) and Burns and Zydney (1999) showed that data for protein transmission through polyethersulfone membranes was in reasonably good agreement with predictions using the centerline approximation of Smith and Deen (1980), although there were significant discrepancies at very low ionic strengths. Causserand et al. (1996) compared their model with data for $\alpha$-lactalbumin sieving, with the model calculations accounting for the presence of a log-normal pore-size distribution in the membrane. However, none of these studies has examined the model predictions under conditions where the proteins and membrane are oppositely charged, and in most cases the model calculations were performed without appropriate independent measurements of the membrane pore-size distribution and/or the membrane surface charge characteristics.

The objective of this study was to quantitatively compare predictions of available theoretical models with experimental data for protein transport under conditions with both attractive and repulsive electrostatic interactions. Experiments were performed using ovotransferrin as a model protein, with the protein charge evaluated as a function of solution pH from available titration data. Sieving data were obtained with both positively and negatively charged polyethersulfone membranes. The membrane surface charge was evaluated from streaming potential measurements, and the membrane pore-size characteristics were determined from sieving data obtained with polydisperse dextrans. This allowed a direct comparison to be made between the experimental data and model predictions.

## Theory

As discussed by Pujar and Zydney (1994), the solute flux through a charged membrane can be expressed as the sum of the convective, diffusive, and electrophoretic contributions

$$N_s = K_c \bar{V} C_s - K_d D_\infty \frac{dC_s}{dz} - K_e u_E E_z C_s \qquad (1)$$

where $C_s$ is the radially averaged solute concentration in the pore, $\bar{V}$ is the radially averaged solution velocity, $D_\infty$ is the free solution Brownian motion diffusivity, $u_E$ is the electrophoretic mobility, and $E_z$ is the streaming potential. $K_c$, $K_d$, and $K_e$ are the hindrance factors for convective, diffusive, and electrophoretic transport, respectively. The diffusive and electrophoretic contributions to protein transport were both negligible under the conditions examined in this study. The hindrance factor for convection can be expressed as an integral over the pore radius (Pujar and Zydney, 1994)

$$K_c = \frac{\int_0^{1-\lambda} GV(\beta) \exp\left(-\frac{\psi_E(\beta)}{k_B T}\right) \beta d\beta}{\left[\int_0^{1-\lambda} \exp\left(-\frac{\psi_E(\beta)}{k_B T}\right) \beta d\beta\right]\left[2\int_0^1 V(\beta)\beta d\beta\right]} \qquad (2)$$

where $\lambda$ is the ratio of the solute to pore radii, $\psi_E(\beta)/k_B T$ is the dimensionless electrostatic energy of interaction, and $\beta$ is the dimensionless radial position in the pore. The exponential terms in the integrals arise from the Boltzmann distribution for the radial concentration profile. The upper limits in these integrals are fixed at $\beta = 1-\lambda$ to account for the steric exclusion of the solute from the region within one solute radius of the pore wall. The lag coefficient ($G$) accounts for the hydrodynamic interactions between the solute and pore walls and is a complex function of the solute and pore size, the solute position in the pore, and the presence of any long-range interactions (see Appendix).

The expression for $K_c$ is often simplified by evaluating $G$ and $\psi_E$ using their values at $\beta = 0$, typically referred to as the centerline approximation (Deen, 1987). Under these conditions, the hindrance factor for convection becomes

$$K_c = \frac{G\int_0^{1-\lambda} V(\beta)\beta d\beta}{2\int_0^1 V(\beta)\beta d\beta} = G\left[2-(1-\lambda)^2\right] \qquad (3)$$

where the final expression is developed assuming Poiseuille (parabolic) flow within the pore.

The solute flux across the membrane can be calculated in terms of the external solute concentrations by integrating Eq. 1 over the membrane thickness. The concentrations just inside the membrane at $z = 0$ and $z = \delta_m$ are expressed in terms of the external concentrations ($C_w$ and $C_f$) using the equilibrium partition coefficient

$$\phi = \frac{C_{s,z=0}}{C_w} = 2\int_0^{1-\lambda} \exp\left[-\frac{\psi_E(\beta)}{k_B T}\right] \beta d\beta \qquad (4)$$

The results are conveniently expressed in terms of the actual sieving coefficient

$$S_a = \frac{C_f}{C_w} = \phi K_c \qquad (5)$$

where $C_f$ and $C_w$ are the solute concentrations in the filtrate and in the solution immediately upstream of the membrane surface. The second expression in Eq. 5 is valid at high filtration velocities where the solute flux is dominated by convection (Pujar and Zydney, 1994).

The electrostatic energy of interaction for a charged spherical solute in a charged cylindrical pore has been evaluated

by Smith and Deen (1980, 1983). The final result for interactions at constant surface charge is conveniently expressed as

$$\frac{\psi_E}{k_B T} = \left( A_s \sigma_s^2 + A_p \sigma_p^2 + A_{sp} \sigma_s \sigma_p \right) / A_{\text{den}} \tag{6}$$

where $A_s$, $A_{sp}$, $A_p$, and $A_{\text{den}}$ are all positive coefficients which depend on the solution ionic strength, the pore radius, the solute radius, and the solute radial position in the pore. Detailed expressions for the coefficients are provided in the Appendix. Similar expressions are available for interactions at constant surface potential (Smith and Deen, 1983) and for interactions with linearized charge regulation boundary conditions (Pujar and Zydney, 1997). The dimensionless surface charge densities of the solute ($\sigma_s$) and pore wall ($\sigma_p$) are

$$\sigma_s = \frac{F r_p q_s}{\epsilon_o \epsilon_r RT} \tag{7}$$

$$\sigma_p = \frac{F r_p q_p}{\epsilon_o \epsilon_r RT} \tag{8}$$

where $\epsilon_o$ is the permittivity of free space, $\epsilon_r$ is the dielectric constant of the solution, $F$ is the Faraday constant, $R$ is the ideal gas constant, and $T$ is the absolute temperature. $q_s$ and $q_p$ are the dimensional values of the surface charge densities of the solute and pore wall, respectively.

The first term in Eq. 6 is associated with the energetic penalty caused by the distortion of the electrical double layer surrounding the protein resulting from the presence of the pore wall. This repulsive interaction is present even when the membrane has no electrical charge. The second term in Eq. 6 is associated with the distortion of the electrical double layer adjacent to the membrane pore walls caused by the finite size of the protein. These first two terms are always repulsive in nature, that is, they cause an increase in the potential energy and a corresponding reduction in the equilibrium partition coefficient. The third term in Eq. 6 accounts for direct charge-charge interactions between the protein and the pore, and is attractive (that is, negative) whenever the protein and pore have opposite (fixed) surface charge.

## Experimental Procedures

KCl solutions were prepared by dissolving pre-weighed amounts of KCl (EM Science, Gibbstown, NJ) in deionized distilled water obtained from a Nanopure water purification system (Barnstead, Dubuque, IA) with resistivity greater than 18 MΩ-cm. These solutions were prefiltered through 0.2 $\mu$m pore size Supor-200 membranes (Gelman Sciences, Inc., Ann Arbor, MI) to remove any particles prior to use. Ovotransferrin (Sigma C 7786) with an isoelectric point (pI) of 5.5 and a molecular weight of 80 kD was obtained from Sigma Chemical (St. Louis, MO). Solutions were prepared by dissolving the powdered protein in the desired KCl solution. The pH was then adjusted by adding small amounts of either HCl or KOH as required, with the pH measured to within 0.01 pH units using an Acumet 915 pH meter (Fisher Scientific, Pittsburgh, PA). Protein solutions were stored at 4°C and used within 3 days of preparation. All protein solutions were filtered through 0.22 $\mu$m syringe filters (Costar Corp., Cambridge, MA) to remove any particles or protein aggregates immediately prior to use.

Protein concentrations were determined using the micro-protein-PR total protein assay (Sigma). A 20 $\mu$L sample was added to 1 mL of reagent, and the absorbance of the resulting complex was measured at 600 nm using a Perkin-Elmer Lambda 4B spectrophotometer (Perkin-Elmer, Norwalk, CT). Protein concentrations were determined by comparison of the absorbance with standard solutions of known concentration.

Filtration experiments were performed using either standard 100,000 molecular weight cutoff Biomax polyethersulfone membranes (Biomax) or prototype 100,000 molecular weight cutoff Biomax positively charged membranes (Biomax$^+$). The latter was produced by chemical modification of the base polyethersulfone using a quaternary amine functionality. These polyethersulfone membranes have an asymmetric structure with the permselective skin layer being about 0.5 $\mu$m in thickness. Both membranes were provided by Millipore Corporation (Bedford, MA) in the form of large flat sheets. Individual membrane disks (25 mm in diameter) were cut using a specially designed cutting device fabricated in our laboratory. Each membrane was flushed with at least 100 L of 0.2 $\mu$m-prefiltered deionized distilled water per m$^2$ of membrane area to remove any wetting agents. The membrane was then soaked for approximately 24 h at 4°C in a 3 g/L solution of ovotransferrin at a pH equal to the protein isoelectric point. Exposure to the protein at its pI provided maximum levels of protein adsorption. This minimized any additional adsorption or fouling during the subsequent protein filtration. The membrane was then gently rinsed with 0.01 M KCl at pH 7 to remove any labile protein prior to use.

### *Protein filtration*

All filtration experiments were conducted in a 25 mm diameter Amicon stirred ultrafiltration cell (Model 8010, Amicon Corp.). The filtration velocity was set by connecting a Rabbit-Plus peristaltic pump (Rainin Instrument Co., Inc., Emeryville, CA) to the filtrate line. Filtrate flow rates were measured by timed collection with the filtrate mass determined using a Sartorius digital balance with accuracy of 1 mg (Model 1518 Sartorius, Westbury, NY).

The stirred cell was initially filled with 0.01 M KCl taking care to remove all trapped air bubbles from the cell and tubing. The stirrer speed was adjusted to 600 rpm using a Strobotac Type 1531-AB strobe light (General Radio Co., Concord, MA). The membrane hydraulic permeability:

$$L_p = \frac{\eta J_v}{\Delta P} \tag{9}$$

was evaluated from the slope of data for the filtrate flux ($J_v$) as a function of applied pressure ($\Delta P$) using at least three data points between 3.5 and 9.7 kPa. The solution viscosity ($\eta$) was evaluated at the system temperature using the empirical correlation presented in the *Handbook of Chemistry and Physics (58th Edition)*. The stirred cell was then emptied and refilled with a protein solution at the desired ionic strength and pH. The stirrer was reset and the filtrate flow rate ad-

justed to 3.6 $\mu$m/s. A minimum of 500 $\mu$L of filtrate was flushed through the membrane to ensure equilibrium operation and to wash out the dead volume downstream of the membrane. At this point, a 100 $\mu$L sample of filtrate was collected. The filtrate port was then clamped and a small (approximately 100 $\mu$L) sample of the bulk solution was obtained directly from the stirred cell. The stirred cell was then carefully emptied, rinsed with 0.01 M KCl, and refilled with a fresh protein solution at a new ionic strength or pH. After completion of the protein filtration, the membrane hydraulic permeability was reevaluated. All experiments were performed at room temperature ($22 \pm 3$°C).

### *Membrane Characterization*

*Membrane Pore Size.* Although the actual pore-size distribution of ultrafiltration membranes is not available, a number of previous studies have used the log-normal density function to characterize the pore-size distribution and evaluate its effect on membrane transport (Zydney et al., 1994). The log-normal probability density function is particularly useful because it is defined only for positive values of the pore radius. It is most convenient to express the results explicitly in terms of the mean ($r_{\text{mean}}$) and standard deviation ($\sigma$) of the distribution

$$f_R(r_p) = \frac{1}{r_p\sqrt{2\pi b}} \exp\left[ - \frac{\left\{ \ln\left( \frac{r_p}{r_{\text{mean}}} \right) + \frac{b}{2} \right\}^2}{2b} \right] \quad (10)$$

where $f_R(r_p)$ is the derivative of the cumulative distribution function and is thus equal to the number of pores between $r_p - \Delta r$ and $r_p + \Delta r$ divided by $2\Delta r$ in the limit as $\Delta r$ goes to zero (Zydney et al., 1994). The parameter $b$ is given as

$$b = \ln\left[ 1.0 + \left( \frac{\sigma}{r_{\text{mean}}} \right)^2 \right] \quad (11)$$

The membrane sieving coefficient can thus be evaluated as

$$\overline{S} = \frac{\int_0^\infty n(r_p) S_a \overline{V} \pi r_p^2 dr_p}{\int_0^\infty n(r_p) \overline{V} \pi r_p^2 dr_p} \quad (12)$$

where $S_a$ is given by Eq. 5 and $\overline{V}$ is given by Poiseuille's equation.

The pore-size distribution in the Biomax membranes was evaluated from dextran sieving measurements. Data were obtained with a mixture of polydisperse dextrans prepared by combining equal amounts of 19,500, 39,200, 70,000, and 147,000 weight-average molecular weight dextrans, all of which were obtained from Sigma Chemical. The dextrans were dissolved in phosphate buffer (0.15 M ionic strength, pH 7.4) prepared from 0.536 g of $Na_2HPO_4 \cdot 7H_2O$, 0.272 g of $KH_2PO_4 \cdot H_2O$, and 0.045 g of NaOH in 1 L of deionized water. Dextran concentrations were determined by size-exclusion chromatography using a TSK-gel G3000 SW silica resin. Column calibration was done using narrow molecular mass dextran standards (11000, 20000, 79000, 97000, and 165000) obtained from American Polymer Standards (Mentor, OH). The column was first equilibrated with fresh buffer at a flow rate of approximately 0.8 mL/min using at least two column volumes. This also served to flush both the sample and reference cells in the refractive index (RI) detector. Column equilibration was confirmed by tracking the base line refractive index. All samples were fed to the SEC system using an AS-400 auto-sampler (Hitachi, Columbia, MD). Dextran detection was done using an LC-30 RI detector (Perkin-Elmer). Data collection was performed using a PE Nelson 900 Series Interface (Perkin-Elmer) connected to a Gateway 2000/386 computer.

Values of $r_{\text{mean}}$ and $\sigma$ were determined by minimizing the sum of the squared residuals between the dextran sieving data and model calculations. At the high salt concentration used in these experiments, the actual dextran sieving coefficient could be evaluated assuming purely steric interactions, that is

$$S_{a,\text{steric}} = (1-\lambda)^2\left[2-(1-\lambda)^2\right] G(\lambda,0) \quad (13)$$

with $G(\lambda,0)$ given in the Appendix. $\overline{S}$ was then evaluated from Eq. 12 with $S_a$ given by Eq. 13. All integrals were evaluated numerically on a SUN computer using available IMSL routines.

*Membrane Charge.* The membrane charge was evaluated from streaming potential measurements following the procedure described by Burns and Zydney (2000). The membrane was sealed between two Plexiglas chambers which were then filled with a 10 mM KCl solution. The solution conductivity was measured using an ES-12 conductivity meter (Horiba, Kyoto, Japan). After carefully removing any entrapped air bubbles, the system was pressurized by adjusting the height of the solution (feed) reservoir. The system was allowed to stabilize for approximately 20 min at which point the transmembrane voltage ($E_z$) was measured using a high impedance 8060A True RMS Multimeter (Fluke Corporation, Everett, WA) connected to the two electrodes. Data were obtained at several pressures in order to evaluate the streaming potential. The device was then rinsed and refilled with fresh KCl solution at a different pH and/or ionic strength. Experiments were performed with both the clean and protein-adsorbed membranes to evaluate any changes in surface charge characteristics associated with exposure to the protein.

The membrane surface charge density was evaluated from the slope of the voltage as a function of pressure as (Saksena and Zydney, 1995)

$$\frac{dE_z}{d\Delta P} = \left( \frac{q_p}{\kappa\eta} \right) B \quad (14)$$

where $q_p$ is the dimensional membrane surface charge density, $\eta$ is the solution viscosity, and $\kappa^{-1}$ is the Debye length

$$\kappa^{-1} = \left[ \frac{F^2}{\epsilon_o \epsilon_r RT} \sum z_i^2 C_i \right]^{1/2} \quad (15)$$

with $z_i$ and $C_i$ the valence and concentration of each ion. The parameter $B$ accounts for the pore-size distribution and is given as (Saksena and Zydney, 1995)

$$B = \frac{\int_0^\infty \frac{I_2(\kappa r_p)}{I_1(\kappa r_p)} f_R(r_p)\pi r_p^2 dr_p}{\int_0^\infty \left[\Lambda_o + \frac{q_p^2}{\eta}\left\{1 - \frac{I_o(\kappa r_p) I_2(\kappa r_p)}{I_1^2(\kappa r_p)}\right\}\right] f_R(r_p)\pi r_p^2 dr_p} \tag{16}$$

where $\Lambda_o$ is the solution conductivity and $I_0$, $I_1$, and $I_2$ are modified Bessel functions of the first kind of orders zero, one, and two, respectively. The membrane surface charge density was calculated iteratively from Eqs. 14–16 using the experimentally measured values of $dE_z/d\Delta P$ and the pore-size distribution $f_R(r_p)$ determined from the dextran sieving data.

## Results

Experimental data for the observed sieving coefficient of ovotransferrin through the Biomax and Biomax$^+$ membranes are shown in Figure 1 as a function of solution pH at both high (500 mM KCl) and low (10 mM KCl) ionic strength. The data were all obtained with 1 g/L solutions of the protein using the same membrane for both the low and high ionic strength experiments. In each case, the data were obtained by monotonically increasing the solution pH with the flux maintained at $J_v = 3.6\times10^{-6}$ m/s using the roller pump. The hydraulic permeability of the membranes decreased by less than 10% over the course of the experiment, indicating that protein fouling was minimal. The observed sieving coefficient ($S_o$) was calculated as the ratio of the protein concentration in the filtrate to that in the bulk solution. The observed sieving coefficients for the Biomax membrane were uniformly smaller than those for the Biomax$^+$ membrane except for a single data point at pH 4.5. The observed sieving coefficient in the 10 mM KCl solution shows a distinct maximum at pH 5.5 for the Biomax membrane and at pH 6.3 for the Biomax$^+$ membrane. The maximum in the sieving coefficient with the Biomax membrane occurs exactly at the isoelectric pH of ovotransferrin, with the maximum value being similar to that obtained using the 500 mM KCl solution. This maximum thus reflects the sieving behavior in the absence of any significant electrostatic interactions. In contrast, the maximum value of the sieving coefficient for the Biomax$^+$ membrane in 10 mM KCl ($S_o = 0.7$) was significantly larger than the values obtained at high ionic strength ($S_o = 0.46$), and the location of this maximum was shifted to a pH > pI, that is, to conditions where the protein has a net negative charge.

To compare the sieving results with the model calculations, it was first necessary to evaluate the pore size and surface charge characteristics of the Biomax membranes. The pore-size distribution was evaluated from dextran sieving measurements. The observed sieving coefficients at $J_v = 3.6\times10^{-6}$ m/s for several distinct dextran fractions are shown as the filled symbols in Figure 2. The results are plotted as a function of the Stokes-Einstein radius of each dextran

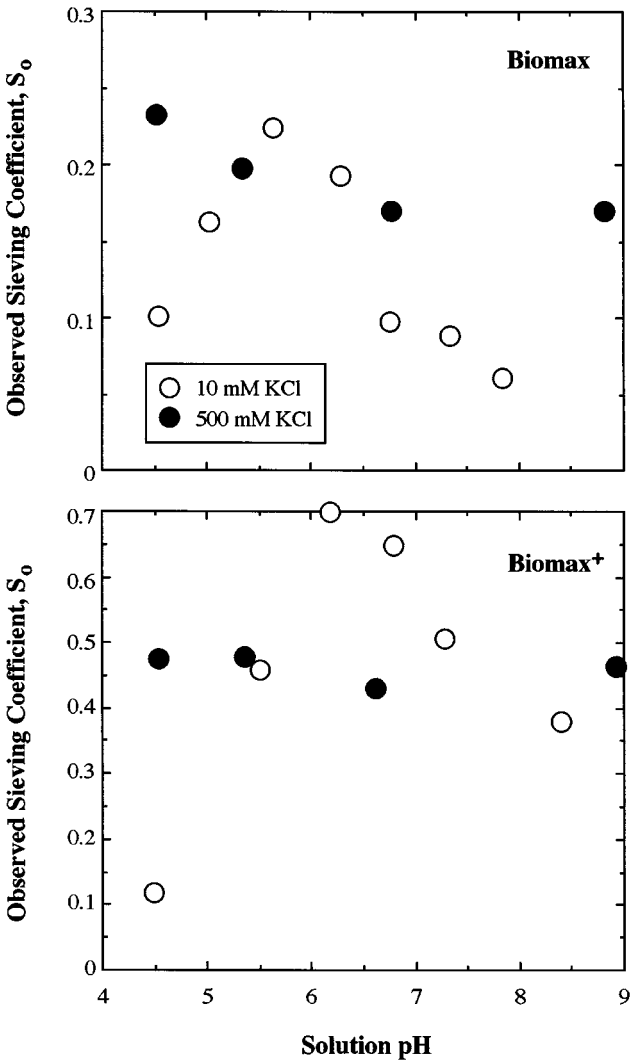


**Figure 1. Observed sieving coefficient as a function of solution pH for the Biomax (upper panel) and Biomax$^+$ (lower panel) membranes.**

Open symbols represent sieving in 10 mM KCl. Filled symbols represent sieving in 500 mM KCl.

$$R_{SE} = \frac{k_B T}{6\pi\eta D_\infty} \tag{17}$$

with the dextran diffusion coefficient $D_\infty$ evaluated from the dextran molecular weight using the correlation developed by Granath and Kvist (1967) based on diffusion data obtained by Granath (1958)

$$\log D_\infty = -4.1154 - 0.47752 \log (\mathrm{MW}) \tag{18}$$

The observed sieving coefficient data were used to evaluate the actual dextran sieving coefficients $S_a = C_f/C_w$ by accounting for the effects of concentration polarization on dex-

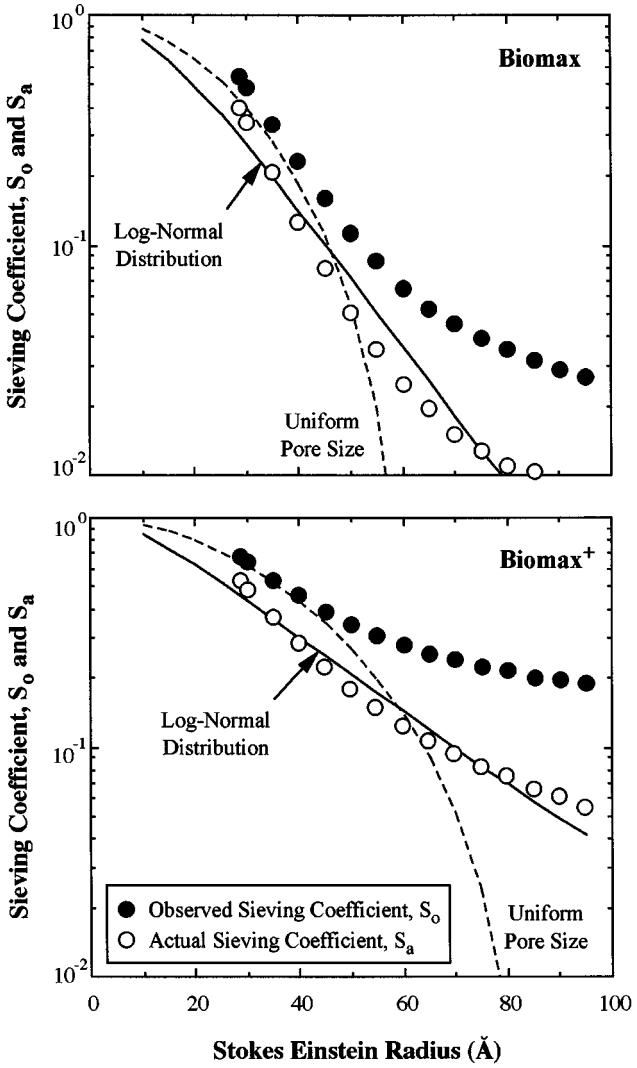


**Figure 2. Observed (filled symbols) and actual (open symbols) sieving coefficients for different dextran fractions through the Biomax (upper panel) and Biomax$^+$ (lower panel) membranes at a flux of $3.6\times10^{-6}$ m/s.**

The solid curves show the model fits to the actual sieving coefficient data with the best fit values of the model parameters shown in Table 1. The dashed curves are the model fits assuming a single pore size for each membrane.

tran transport in the bulk solution

$$S_a = \frac{S_o}{(1-S_o)\exp\left(\frac{J_v}{k}\right)+S_o} \tag{19}$$

Equation 19 is developed using a simple stagnant film model (Blatt et al., 1970), with the average mass-transfer coefficient in the stirred cell ($k$) calculated as (Smith et al., 1968)

$$\frac{kr_c}{D_\infty} = \chi(Re)^{0.567}(Sc)^{0.33} \tag{20}$$

**Table 1. Membrane Pore-Size Characteristics**

| Membrane | Mean Pore Size $r_{mean}$ (m) | Std. Dev. $\sigma/r_{mean}$ | Uniform Pore Size $r_p$ (m) |
|---|---|---|---|
| Biomax | $3.0\times10^{-9}$ | 0.42 | $6.5\times10^{-9}$ |
| Biomax$^+$ | $2.4\times10^{-9}$ | 0.60 | $9.0\times10^{-9}$ |

where $Re=\omega r_c^2/\nu$ is the Reynolds number, $Sc=\nu/D_\infty$ is the Schmidt number, $r_c$ is the radius of the stirred cell, $\omega$ is the stirring speed, $D_\infty$ is the solute diffusivity (evaluated using Eq. 18 for each dextran), and $\nu$ is the kinematic viscosity. The coefficient $\chi$ is a function of device geometry and was evaluated as $\chi=0.23$ by Opong and Zydney (1991) for the Model 8010 stirred cell.

The best fit values of the mean pore radius and the standard deviation in the log-normal distribution were determined by minimizing the sum of squared residuals between the logarithms of the actual sieving coefficient data and the model calculations. The model calculations are shown as the solid curves, with the best fit values of the parameters summarized in Table 1. The overall fits to the data are quite good, suggesting that the log-normal density function provides a reasonable description of the pore-size distribution of these membranes. Interestingly, the best fit value of the mean pore size for the Biomax$^+$ membrane is somewhat smaller than that for the Biomax membrane even though the dextran sieving coefficients are larger. This can be explained by the greater value of the standard deviation in the pore size of the Biomax$^+$ membrane ($\sigma=1.44\times10^{-9}$ m) compared to that for the Biomax membrane ($\sigma=1.26\times10^{-9}$ m) with the sieving behavior strongly influenced by the flow through the larger pores in the distribution. The differences in pore-size distribution are due to the inherent variability between membranes in combination with the effects of the surface modification used to produce the Biomax$^+$ membrane. Also shown for comparison are model fits assuming a single pore size (dashed curve) using the best fit values of $r_p=6.5\times10^{-9}$ m for the Biomax and $r_p=9.0\times10^{-9}$ m for the Biomax$^+$. The calculations using a single pore size provide a poor overall fit to the data, significantly overpredicting $S_a$ for the smaller dextrans and underpredicting $S_a$ for the larger dextrans.

Figure 3 shows the membrane surface charge density for the Biomax (top panel) and Biomax$^+$ (bottom panel) membranes as a function of pH as determined from streaming potential data ($dE_z/d\Delta P$) obtained with 10 mM KCl using Eqs. 14–16. Data are shown for the membranes both before and after exposure to ovotransferrin. The solid curves are spline fits to the data. The results for the clean membrane have been discussed in more detail elsewhere (Burns and Zydney, 2000). The clean Biomax membrane is negatively charged at pH above ~2.5, reaching a value of $q_p=-7.0\times10^{-3}$ C/m$^2$ at pH 6.5. Exposure to ovotransferrin causes the isoelectric point of the Biomax membrane to shift to pH 5.5, which almost exactly coincides with the isoelectric point of the protein. Similar behavior has been reported by Causserand et al. (1994) for adsorption of bovine serum albumin on sulfonated polysulfone ultrafiltration membranes. The Biomax$^+$ membrane is positively charged over the entire pH range with the charge slowly decreasing from $q_p=1.0\times10^{-2}$ C/m$^2$ at pH 3.5 to $q_p=0.55\times10^{-2}$ C/m$^2$ at pH 10. Expo-

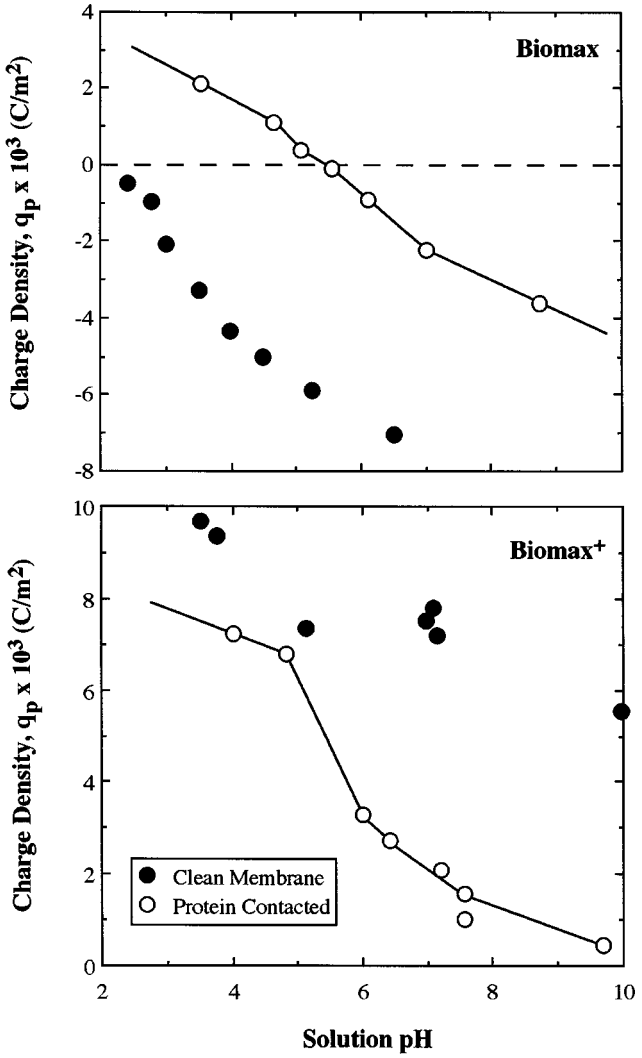


**Figure 3. Surface charge density of the Biomax (top panel) and Biomax$^+$ (bottom panel) membranes in 10 mM KCl both before (filled symbols) and after (open symbols) exposure to ovotransferrin.**

Solid curves are simple spline fits to the data.

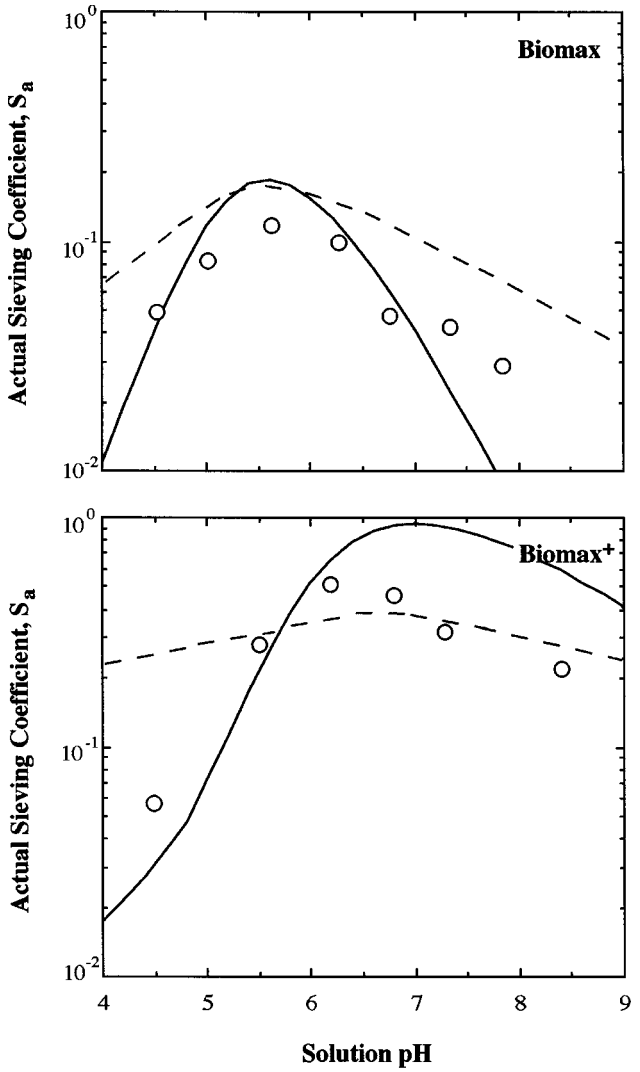


**Figure 4. Actual sieving coefficient for ovotransferrin through the Biomax (top panel) and Biomax$^+$ (bottom panel) membranes in 10 mM KCl.**

Solid curves are model calculations using the complete solution for $\psi_E(\beta)$. Dashed curves are model calculations using the centerline approximation.

sure to ovotransferrin causes a reduction in the surface charge density of the Biomax$^+$ membrane, particularly at pH values above the protein isoelectric point where the protein and membrane are oppositely charged. This reduction in charge is caused by the reversible binding of the negatively charged ovotransferrin to the positively charged membrane.

The ovotransferrin sieving data from Figure 1 are compared with the model calculations in Figure 4. The data have been plotted as the actual sieving coefficients, which were evaluated directly from the observed sieving data using Eqs. 19 and 20 with $D_\infty = 5.7\times10^{-7}$ cm$^2$/s as determined from the correlation developed by Young et al. (1980). All calculations were done using the pore-size distribution parameters evaluated from the dextran sieving data (values in Table 1). The protein radius was evaluated as $r_s = 3.75\times10^{-9}$ m using the Stokes-Einstein equation. This radius was assumed to be constant over the range of pH and ionic strength examined in this study, consistent with results from intrinsic viscosity measurements (Tanford and Buzzell, 1956). The surface charge density of ovotransferrin was evaluated at each pH from the $pK_a$ values of the different ionizable groups (Table A3) as will be discussed in the Appendix. The surface charge density of the membrane was evaluated from the spline fits shown in Figure 3.

The solid and dashed curves in Figure 4 represent the model calculations, with the sieving coefficient evaluated from Eq. 12 by integrating over the log-normal pore-size distribution. The equilibrium partition coefficient was evaluated from Eq. 4 with the energy of interaction calculated using Eq. 6. Two different expressions were used for $\psi_E(\beta)$: (1) the complete solution developed by Smith and Deen (1983), with results shown as solid curves; (2) the centerline approximation

in which $\psi_E(\beta)$ was assumed to be equal to $\psi_E(\beta = 0)$, with the results shown as dashed curves. The coefficients $A_s$, $A_p$, $A_{sp}$, and $A_{\text{den}}$ for the two analyses are given in the appendix in Table A1. In both cases the upper limit on the integral in Eq. 4 was modified to account for the presence of the Born layer using a thickness of $1.57 \times 10^{-10}$ m, as reported by Bhattacharjee and Sharma (1995). The model calculations thus involve no adjustable parameters. All the physical constants associated with the membrane ($q_p$, $r_{\text{mean}}$, $\sigma$) and protein ($q_s$, $r_s$) were determined from independent experimental measurements.

The experimental data for the actual sieving coefficient for both the Biomax and the Biomax$^+$ membranes are in good agreement with the model calculations using the complete solution for the energy of interaction. The model accurately predicts the location of the maximum value of $S_a$ for the Biomax membrane at pH 5.5 (equal to the isoelectric point for ovotransferrin), and also qualitatively predicts the shift in the maximum value to a pH greater than the pI for the Biomax$^+$ membrane. The model also correctly predicts that $S_o$ for the Biomax$^+$ membrane at $5.5 < \text{pH} < 7.5$ is greater than that at high ionic strength (that is, in the absence of electrostatic interactions). The model is in very good agreement with the data at the lower pH, but tends to overpredict the data for the Biomax$^+$ membrane at the higher pH. The possible cause for this discrepancy at higher pH is discussed in more detail subsequently.

The model calculations using the centerline approximation for $\psi_E$ are in much poorer agreement with the data. The calculations for the Biomax membrane show the correct qualitative dependence on pH, but the model significantly overpredicts the sieving coefficients at both high and low pH. This behavior is a direct result of the centerline approximation. The energy of interaction between the protein and pore wall is smallest when the solute is located at the pore axis, thus the assumption that $\psi_E$ remains constant at its centerline value will significantly underestimate the magnitude of the electrostatic interactions. The model calculations for the Biomax$^+$ membrane significantly overpredict the sieving coefficient at the lowest pH where the protein and membrane have like charge, but the results are in fairly good agreement with the data at high pH where the protein and membrane are oppositely charged. This behavior is discussed in more detail subsequently.

In order to understand the origin of the pH dependence seen in Figure 4, it is useful to examine the different contributions to the energy of interaction (Eq. 6). This is difficult to do quantitatively because of the required integrations over the pore radius (to evaluate the partition coefficient) and then over the pore-size distribution (to evaluate the actual sieving coefficient). The relative importance of the different contributions were thus estimated by evaluating $S_a$ using the complete solution for $\psi_E$ but only accounting for one of the three terms in the expression for the energy of interaction (Eq. 6). The results are shown in Figure 5 along with the experimental data for the actual sieving coefficients for the Biomax and Biomax$^+$ membranes. Corresponding calculations for the average solute partition coefficient, determined by integrating the expression for $\phi$ over the pore-size distribution, show identical trends to the $S_a$ results since the hindrance factor for convection is only a very weak function of the protein or

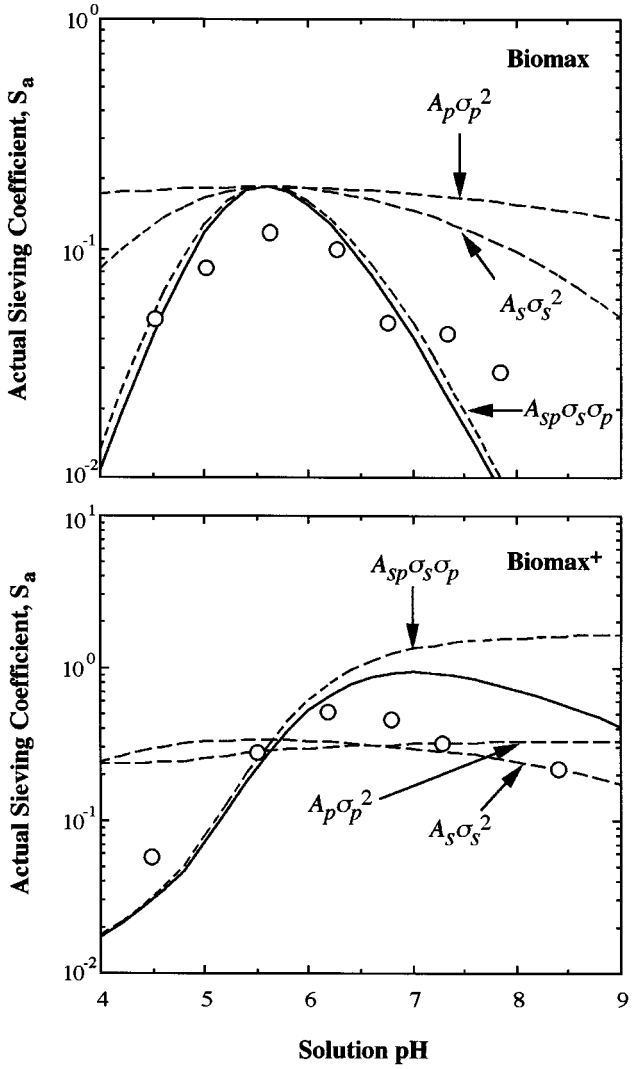


**Figure 5. Calculated values of the actual sieving coefficient accounting for different contributions to the total electrostatic energy of interaction for ovotransferrin sieving through the Biomax (top panel) and Biomax$^+$ (bottom panel) membranes.**

membrane charge. The contribution from the $A_p\sigma_p^2$ term is quite small for both membranes, thus the model calculations for $S_a$ are nearly independent of pH under these conditions. The dominant contribution to the electrostatic energy arises from the direct charge-charge interaction and is proportional to $\sigma_s\sigma_p$. This term is repulsive at essentially all pH for the Biomax membrane since the charge on the ovotransferrin and the membrane are of like sign throughout almost the entire pH range. In contrast, the charge-charge interaction for the Biomax$^+$ membrane is attractive at $5.5 < \text{pH} < 10$ since the protein and membrane are oppositely charged under these conditions. This leads to the observed increase in the protein partition coefficient, and in turn $S_a$. The electrostatic interaction associated with the distortion of the electrical double layer around the protein (proportional to $\sigma_s^2$) is repulsive at all pH. This term adds to the total energy of interaction for

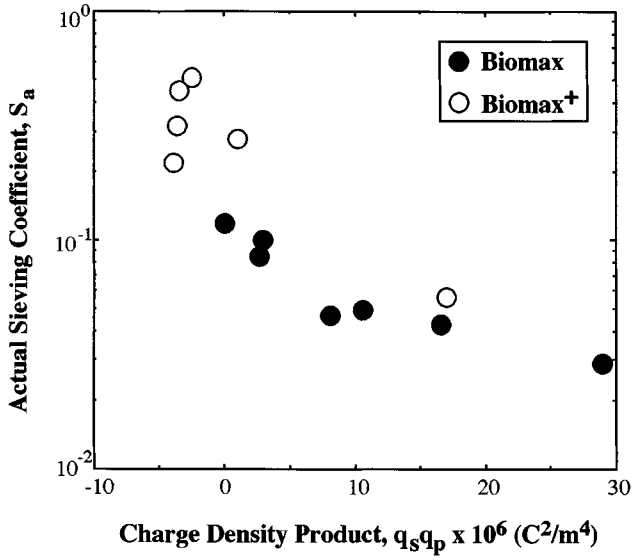


**Figure 6. Actual sieving coefficient as a function of the product of the protein and membrane surface charge densities for ovotransferrin filtration through the Biomax and Biomax$^+$ membranes in 10 mM KCl over a range of pH.**

the Biomax membrane, but it competes against the attractive charge-charge interaction for the Biomax$^+$ membrane at pH $> 5.5$. It is the repulsive interaction arising from the distortion of the double layer that causes the actual sieving coefficient to decrease at high pH for the Biomax$^+$ membrane, even though the attractive charge-charge interaction increases in magnitude throughout the full pH range.

The importance of the charge-charge interactions on protein sieving can be seen more explicitly by replotting the experimental data in terms of the product of the surface charge densities of the protein and pore (Figure 6). The data for the Biomax membrane at both low and high pH collapse to nearly a single line when plotted in this manner. For example, the data at pH 4.5 and 6.8 have very similar values of $q_s q_p$ ($10.5 \times 10^{-6}$ C$^2$/m$^4$ and $8.2 \times 10^{-6}$ C$^2$/m$^4$, respectively) and very similar sieving coefficients ($S_a = 0.049$ and 0.047, respectively), even though the protein and membrane are positively charged at pH 4.5 and are negatively charged at pH 6.8. The results for the Biomax$^+$ membrane show considerably greater scatter in Figure 6, particularly at the negative values of $q_s q_p$. This is due to the large negative charge on the protein at high pH and the importance of the $q_s^2$ term under these conditions.

Figure 7 examines the effects of the membrane pore-size distribution on the model calculations. Results are shown for the complete model, with the pore size evaluated using both the log-normal distribution (solid curve) and with a single pore size (dashed curve). The pore-size parameters were all determined from the dextran sieving data with values given in Table 1. The model calculations using a single pore size are in poor agreement with the experimental data for both the Biomax and the Biomax$^+$ membranes. The model significantly underpredicts the magnitude of the electrical interactions, yielding a much weaker dependence of $S_a$ on solution pH for

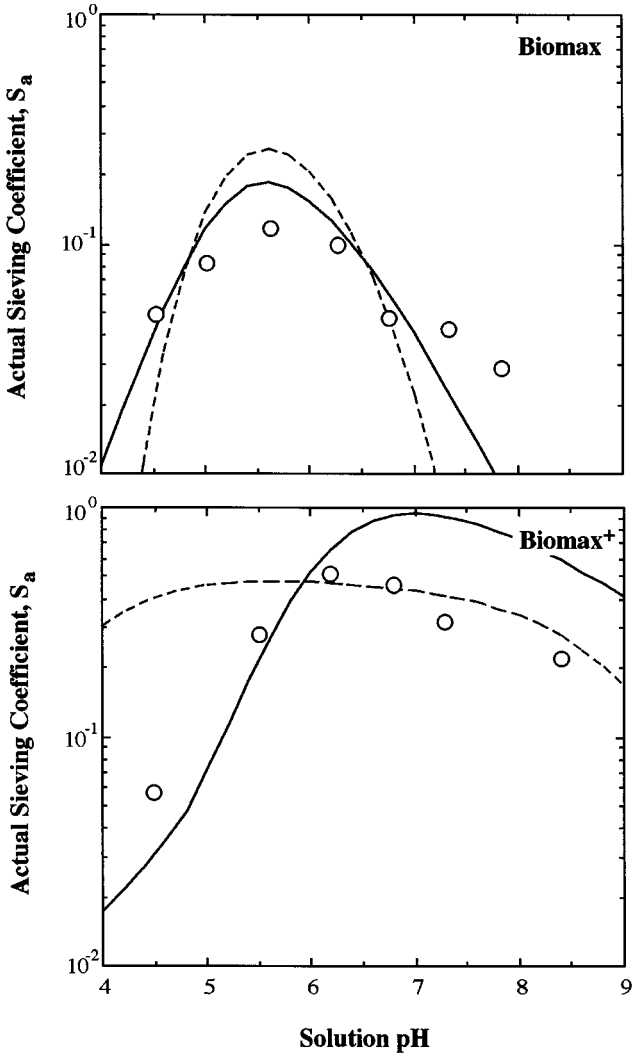


**Figure 7. Effects of pore-size distribution on the actual sieving coefficients for the Biomax (top panel) and Biomax$^+$ (bottom panel) membranes.**

both membranes. In addition, the model calculations for the Biomax membrane are much higher than the data even at the protein isoelectric point, which is a direct result of the large value of the pore size used in the simulations. Better agreement with the data could be obtained using a smaller pore size, but the model then predicts a much sharper pH dependence than seen experimentally or than predicted using the log-normal pore size distribution. The model calculations for the Biomax$^+$ membrane using only a single pore size yielded a maximum value of $S_a$ at pH = pI, with repulsive interactions seen at both low and high pH. The absence of any significant attractive interactions under these conditions was caused by the large reduction in the $\sigma_s \sigma_p$ term, with the energy of interaction now dominated by the distortion of the electrical double layer around the charged protein.

The effect of solution ionic strength on the ovotransferrin sieving coefficients is examined in Figure 8. Experiments were performed using three separate 1 g/L solutions of ovotransferrin, with the pH adjusted to 4.0, 6.5, or 9.0 using either

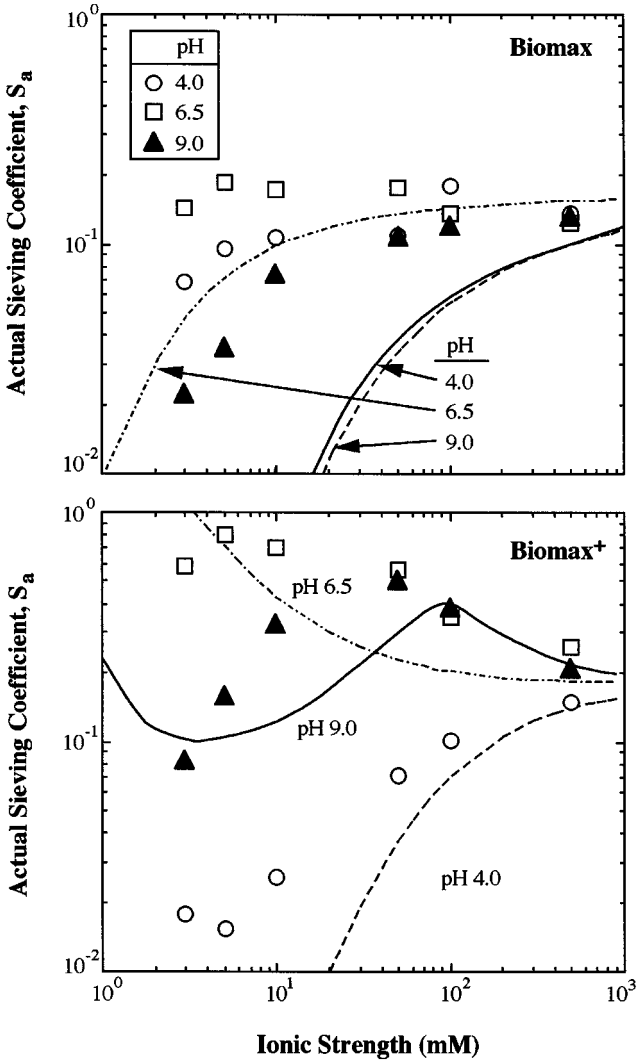


**Figure 8. Actual sieving coefficient for ovotransferrin through a Biomax (top panel) and Biomax$^+$ (bottom panel) membrane as a function of solution ionic strength at three pH values.**

Solid curves are model calculations using the complete solution for $\psi_E(\beta)$.

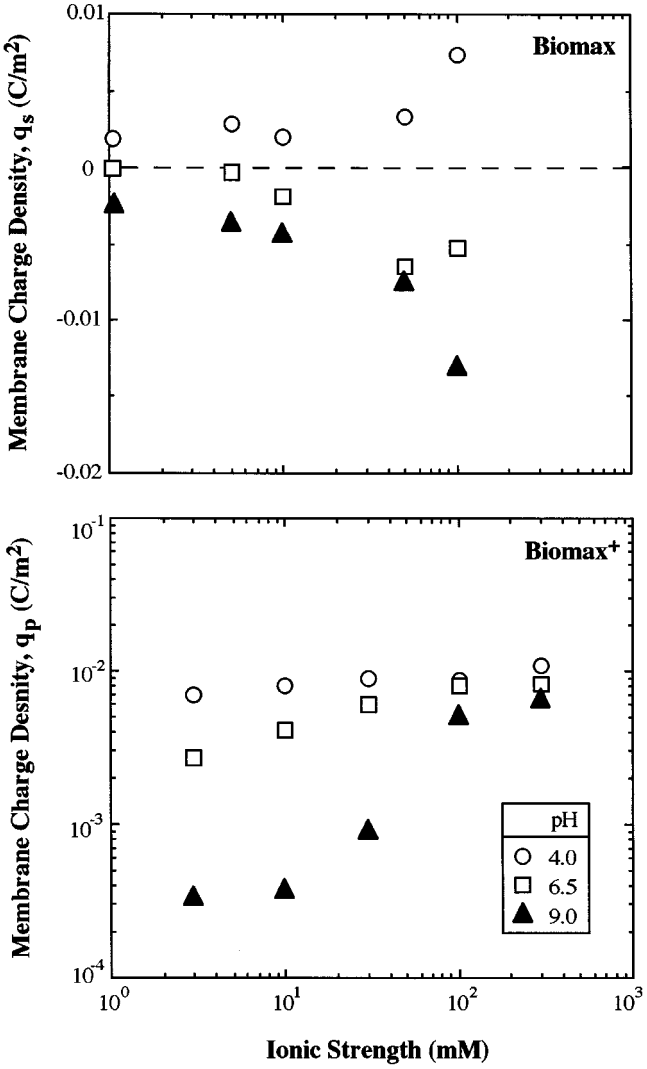


**Figure 9. Membrane surface charge density for the Biomax (top panel) and Biomax$^+$ (bottom panel) membranes as a function of ionic strength at three values of the solution pH.**

HCl or KOH. The data were obtained by monotonically increasing the solution ionic strength, beginning at the lowest value. Results are shown for the actual sieving coefficients, which were again calculated directly from the $S_o$ data using Eqs. 19 and 20. The actual sieving coefficients approach a constant value at high ionic strength due to the absence of any significant electrostatic interactions under these conditions. The $S_a$ values for the Biomax membrane decrease monotonically with decreasing ionic strength, with the magnitude of the interactions being greatest at pH 9.0 due to the large negative charge on both the membrane and the ovotransferrin at this pH. The sieving behavior for the Biomax$^+$ membrane is considerably more complex. The data at pH 4.0 (where the protein and membrane both have a net positive charge) show a monotonic decrease, while the data at pH 6.5 (where the protein and membrane are oppositely-charged) show a monotonic increase in $S_a$. The sieving data at pH 9.0 show a local maximum around 50 mM KCl, with $S_a$ decreasing sharply at ionic strength below 10 mM.

The solid curves in Figure 8 are the model calculations using the complete solution for the energy of interaction, with the membrane surface charge density determined from the streaming potential data shown in Figure 9. The magnitude of the surface charge for the Biomax membrane tended to increase with increasing solution ionic strength, with the charge being negative at pH 6.5 and 9.0 and positive at pH 4.0. The surface charge on the Biomax$^+$ membrane also increased with increasing ionic strength, with the magnitude of the ionic strength dependence being most pronounced at pH 9. The model calculations for the Biomax membrane show the correct qualitative behavior, but significantly overpredict the magnitude of the electrostatic interactions at low ionic strength. Note that the model calculations for the Biomax$^+$ membrane in Figure 8 were performed with $r_{\text{mean}} = 1.7 \times 10^{-9}$ m, compared to $r_{\text{mean}} = 2.4 \times 10^{-9}$ m for the membrane used

in the experiments from Figures 1 and 4, to provide a better fit to the actual sieving coefficients for this particular membrane at the highest ionic strength. The value of $\sigma/r_{mean}$ was maintained at 0.6 as previously determined from the dextran sieving data. The model calculations for the Biomax$^+$ membrane properly capture the very complex dependence on ionic strength seen experimentally. The predicted sieving coefficients at pH 4.0 decrease monotonically with decreasing ionic strength due to the increase in the magnitude of the repulsive interactions between the positively charged protein and the positively charged membrane under these conditions. The attractive interactions between the oppositely charged protein and membrane at pH 6.5 lead to the increase in $S_a$ with decreasing ionic strength seen at pH 6.5. The actual sieving coefficient for the Biomax$^+$ membrane at pH 9.0 is predicted to initially increase with decreasing ionic strength due to the attractive interaction between the oppositely charged protein and membrane. However, the membrane surface charge at pH 9.0 decreases rapidly with decreasing ionic strength (Figure 9), causing the overall energy of interaction to be dominated by the repulsive $\sigma_s^2$ term for ionic strengths between 1.2 and 15 mM. The predicted increase in $S_a$ at pH 9.0 at the very lowest ionic strength arises from the very large increase in the magnitude of the charge-charge interaction term at low ionic strengths, with this term again dominating the energy of interaction for ionic strengths less than 1.2 mM.

## Discussion

The results presented in this study clearly demonstrate that available hydrodynamic and partitioning models can provide a very good description of the effects of electrostatic interactions on the transport of a charged protein through a charged membrane in the presence of both repulsive and attractive interactions. The theoretical calculations were performed with all model parameters evaluated from independent experimental measurements. The membrane pore-size distribution was determined from dextran sieving data. The membrane surface charge density was evaluated from streaming potential measurements. The effective protein radius was determined from the diffusivity of ovotransferrin using the Stokes-Einstein equation. Also, the protein surface charge density was evaluated from a model accounting for the dissociation of the different ionizable amino acid residues in ovotransferrin. The model properly describes the effects of solution pH and ionic strength on protein transmission through both the Biomax and Biomax$^+$ membranes. The model also correctly predicts the local maximum in the protein sieving coefficient at an intermediate ionic strength seen at pH 9.0. This maximum is caused by the different ionic strength dependence of the contributions from direct charge-charge interactions and from the distortion of the electrical double layer around the protein to the overall energy of interaction. Calculations performed using the centerline approximation, which has been used extensively in previous studies of membrane transport, were in fairly good agreement with the experimental data when the interactions were repulsive in nature, although this approximation tended to underpredict the magnitude of the electrostatic interactions.

The good agreement between the model and data in this system is in some ways surprising given the numerous approximations underlying the analysis. In particular, the polyethersulfone membranes used in these experiments have a highly irregular interconnected porous network, which is in sharp contrast to the parallel array of cylindrical pores used in the model. In this case, the complexity of the actual pore-size distribution is accounted for in the analysis by evaluating the mean and standard deviation in the assumed log-normal distribution directly from dextran sieving data using the same hydrodynamic and partitioning models, but in the absence of any electrostatic interactions. This effectively lumps our ignorance of the details of the pore morphology, structure, and distribution into these two geometric parameters. It is important to note that this does not in any way imply that the Biomax membranes actually have a log-normal distribution of pore radii. Instead, the results demonstrate that the sieving characteristics of these asymmetric membranes can be effectively described using this type of probability density function with the mean and standard deviation fit to the dextran sieving data.

The model calculations were also performed assuming that any long-range interactions due to dispersion or van der Waals forces were negligible. The quantitative evaluation of these interactions is difficult due to the absence of accurate data on the Hamaker constant for the ovotransferrin-Biomax membrane system. Zydney and Pujar (1998) have discussed the effects of dispersion forces on protein transport through porous membranes.

The model also assumes that the electrical interactions occur at constant charge density on the protein and pore surfaces. However, the electrical potential field around the protein will be significantly distorted by the presence of the pore boundary. This will cause a change in the local hydrogen ion concentration in the vicinity of the protein surface, thus altering the extent of ionization of the amino acid residues and in turn the magnitude of the protein charge. A similar effect will occur with the pore charge due to the distortion of the electrical potential field near the pore wall associated with the presence of the protein. This phenomenon is often referred to as charge regulation. Pujar and Zydney (1997) evaluated the electrical energy of interaction for a charged sphere in a charged cylindrical pore by solving the linearized Poisson-Boltzmann equation using a linearized form of the charge regulation boundary condition that implicitly accounts for the changes in surface charge density and surface potential caused by the distortion of the electrical potential field. Detailed calculations using this model could not be performed for the ovotransferrin-Biomax membrane system due to the lack of sufficient data on the protein and pore charge needed to evaluate the charge regulation parameters. However, Pujar and Zydney (1997) demonstrated that the charge regulation phenomenon tends to reduce the magnitude of the electrical energy of interaction. This may well explain the overprediction of the ovotransferrin sieving data at pH $> 6$ seen in Figure 4 and some of the discrepancies between the model and data at the different ionic strength seen in Figure 8.

## Acknowledgments

The authors would like to acknowledge the technical and financial support provided by Genentech, Inc. and Millipore Corporation and a grant from the National Science Foundation.

## Notation

$A_{den}$ = coefficient in the energy of interaction equation
$A_p$ = coefficient describing the pore double layer term in the energy of interaction
$A_s$ = coefficient describing the solute double layer term in the energy of interaction
$A_{sp}$ = coefficient describing the solute-pore term in the energy of interaction
$b$ = parameter in the log-normal density function
$B$ = parameter accounting for the pore size distribution in the streaming potential
$C_i$ = concentration of $i$th ion (mol/L)
$C_s$ = radially averaged solute concentration in pore (g/L)
$D_\infty$ = solute diffusivity in free solution ($m^2/s$)
$e$ = electronic charge (C)
$E_z$ = electric field within the membrane (V/m)
$f_R(r_p)$ = probability density function ($m^{-1}$)
$F$ = Faraday's constant (C/mol)
$G$ = hydrodynamic lag coefficient
$J_v$ = filtration flux (m/s)
$k$ = mass transfer coefficient (m/s)
$k_B$ = Boltzmann's constant (J/K)
$K_c$ = hindrance factor for convection
$K_d$ = hindrance factor for diffusion
$K_e$ = hindrance factor for electrophoretic transport
$L_p$ = membrane hydraulic permeability (m)
MW = protein molecular weight (kg/mol)
$N_s$ = solute flux through membrane ($kg/m^2/s$)
$r_c$ = radius of stirred cell (m)
$r_{mean}$ = mean pore radius (m)
$r_p$ = pore radius (m)
$r_s$ = solute radius (m)
$R$ = ideal gas constant (J/mol/K)
$R_{SE}$ = Stokes-Einstein radius (m)
$Re$ = Reynolds number
$q_p$ = pore surface charge density ($C/m^2$)
$q_s$ = solute surface charge density ($C/m^2$)
$\bar{S}$ = mean solute sieving coefficient
$S_a$ = actual solute sieving coefficient
$S_o$ = observed solute sieving coefficient
$Sc$ = Schmidt number
$T$ = absolute temperature (K)
$u_E$ = solute electrophoretic mobility (m/s/V)
$V$ = local fluid velocity in pore (m/s)
$\bar{V}$ = radially averaged fluid velocity in pore (m/s)
$\beta$ = dimensionless radial position in pore
$\Delta P$ = transmembrane pressure drop (Pa)
$\epsilon_o$ = permittivity of free space (C/V/m)
$\epsilon_r$ = dielectric constant of medium
$\eta$ = solution viscosity (P)
$\kappa^{-1}$ = Debye length (m)
$\lambda$ = dimensionless solute radius, $r_s/r_p$
$\Lambda_o$ = bulk solution conductivity (S)
$\nu$ = kinematic viscosity ($m^2/s$)
$\phi$ = solute partition coefficient into pore
$\sigma$ = standard deviation in pore size (m)
$\sigma_p$ = dimensionless surface charge density of pore
$\sigma_s$ = dimensionless surface charge density of solute
$\chi$ = coefficient in mass-transfer correlation
$\psi_E$ = energy of interaction (J)
$\psi_s^*$ = electrical potential at protein surface (J)
$\omega$ = stirrer speed ($s^{-1}$)

## Literature Cited


Balakrishnan, M., and G. P. Agarwal, "Protein Fractionation in a Vortex Flow Filter: I. Effect of System Hydrodynamics and Solution Environment on Single Protein Transmission, *J. Memb. Sci.*, **112**, 47 (1996).

Bhattacharjee, S., and A. Sharma, "Lifshitz-van der Waals Energy of Spherical Particles in Cylindrical Pores," *J. Colloid Interface Sci.*, **171**, 288 (1995).

Blatt, W. F., A. Dravid, A. S. Michaels, and L. Nelson, "Solute Polarization and Cake Formation in Membrane Ultrafiltration: Causes, Consequences, and Control Techniques," *Membrane Science and Technology*, J. E. Flinn, ed., Plenum, New York (1970).

Bungay, P. M., and H. Brenner, "The Motion of a Closely Fitting Sphere in a Fluid Filled Tube," *Int. J. Multiphase Flow*, **1**, 25 (1973).

Burns, D. B., and A. L. Zydney, "Buffer Effects on the Zeta Potential of Ultrafiltration Membranes, *J. Memb. Sci.*, **172**, 39 (2000).

Burns, D. B., and A. L. Zydney, "Effect of Solution pH on Protein Transport through Ultrafiltration Membranes," *Biotechnol. Bioeng.*, **64**, 27 (1999).

Causserand, C., M. Meireles, and P. Aimar, "Protein Transport through Charged Porous Membranes," *Trans. IchemE*, **74**, 113 (1996).

Causserand, C., M. Nystrom, and P. Aimar, "Study of Streaming Potentials of Clean and Fouled Ultrafiltration Membranes," *J. Memb. Sci.*, **88**, 211 (1994).

Deen, W. M., "Hindered Transport of Large Molecules in Liquid-Filled Pores," *AIChE J.*, **33**, 1409 (1987).

Granath, K. A., "Solution Properties of Branched Dextrans," *J. Colloid Sci.*, **13**, 308 (1958).

Granath, K. A., and B. E. Kvist, "Molecular Weight Distribution Analysis by Gel Chromatography on Sephadex," *J. Chromatog.*, **28**, 69 (1967).

Malone, D. M., and J. L. Anderson, "Hindered Diffusion of Particles through Small Pores," *Chem. Eng. Sci.*, **33**, 1429 (1978).

Millesime, L., C. Amiel, and B. Chaufer, "Ultrafiltration of Lysozyme and Bovine Serum Albumin with Polysulfone Membranes Modified with Quaternized Polyvinylimidazole," *J. Memb. Sci.*, **89**, 223 (1994).

Mitchell, B. D., and W. M. Deen, "Effect of Concentration on the Rejection Coefficient of Rigid Macromolecules in Track-Etched Membranes," *J. Colloid Interface Sci.*, **113**, 132 (1986).

Miyama, H., H. Yoshida, and Y. Nosaka, "Negatively Charged Polyacrylonitrile Graft Copolymer Membrane for Permeation and Separation of Plasma Proteins," *Makromol. Chem., Rapid Commun.*, **9**, 57 (1988).

Munch, W. D., L. P. Zestar, and J. L. Anderson, "Rejection of Polyelectrolytes from Microporous Membranes," *J. Memb. Sci.*, **5**, 77 (1979).

Nakao, S., H. Osada, H. Kurata, T. Suru, and S. Kimura, "Separation of Proteins by Charged Ultrafiltration Membranes," *Desalination*, **70**, 191 (1988).

Opong, W., and A. L. Zydney, "Diffusive and Convective Protein Transport through Asymmetric Membranes," *AIChE J.*, **37**, 1497 (1991).

Overbeek, J. T. G., "Electrokinetic Phenomena," *Colloid Science*, H. R. Kruyt, ed., Elsevier, Amsterdam (1952).

Pujar, N. S., and A. L. Zydney, "Electrostatic and Electrokinetic Interactions During Protein Transport through Narrow Pore Membranes," *Ind. Eng. Chem. Res.*, **33**, 2473 (1994).

Pujar, N. S., and A. L. Zydney, "Charge Regulation and Electrostatic Interactions for a Spherical Particle in a Cylindrical Pore," *J. Colloid Interface Sci.*, **192**, 338 (1997).

Saksena, S., and A. L. Zydney, "Pore Size Distribution Effects on Electrokinetic Phenomena in Semipermeable Membranes," *J. Memb. Sci.*, **105**, 203 (1995).

Smith, F. G., and W. M. Deen, "Electrostatic Double-Layer Interactions for Spherical Colloids in Cylindrical Pores," *J. Colloid Interface Sci.*, **78**, 444 (1980).

Smith, F. G., and W. M. Deen, "Electrostatic Effects on the Partitioning of Spherical Colloids between Dilute Bulk Solution and Cylindrical Pores," *J. Colloid Interface Sci.*, **91**, 571 (1983).

Smith, K. A., C. K. Colton, E. W. Merrill, and L. B. Evans, "Convective Transport in a Batch Dialyzer: Determination of the True Membrane Permeability from a Single Measurement," *AIChE Symp. Ser.*, **64**, 45 (1968).

Tanford, C., and J. G. Buzzell, "The Viscosity of Aqueous Solutions of Bovine Serum Albumin Between pH 4.3 and 10.5," *J. Phys. Chem.*, **60**, 225 (1956).

van Reis, R., J. M. Brake, J. Charkoudian, D. B. Burns, and A. L. Zydney, "High-Performance Tangential Flow Filtration using Charged Membranes," *J. Memb. Sci.*, **159**, 133 (1999).

Warner, R. C., and I. Weber, "The Metal Combining Properties of Conalbumin," *J. A. C. S.*, **75**, 5094 (1953).

Williams, J., T. C. Elleman, I. B. Kingston, A. G. Wilkins, and K. A. Kuhn, ''The Primary Structure of Hen Ovotransferrin,'' *Eur. J. Biochem*., **122**, 297 (1982).
Young, M. E., P. A. Carroad, and R. L. Bell, ''Estimation of Diffusion Coefficients of Proteins,'' *Biotech. Bioeng.*, **22**, 947 (1980).
Zydney, A. L., P. Aimar, M. Meireles, J. M. Pimbly, and G. Belfort, ''Use of the Log-Normal Probability Density-Function to Analyze Membrane Pore-Size Distributions: Functional Forms and Discrepancies,'' *J. Memb. Sci.*, **91**, 293 (1994).
Zydney, A. L., and N. S. Pujar, ''Protein Transport Through Porous Membranes: Effect of Colloidal Interactions,'' *Colloids Surfaces. A: Physicochem. Eng. Aspects*, **138**, 133 (1998).

## Appendix

Smith and Deen (1980, 1983) evaluated the electrostatic energy of interaction for a charged spherical solute in a charged cylindrical pore by solving the linearized Poisson-Boltzmann equation by matching solutions in both cylindrical and spherical coordinates. Calculations were originally performed for a solute located at the pore axis ($\beta = 0$). These were subsequently extended to arbitrary radial positions. In both cases, the dimensionless energy of interaction for constant surface charge density was given as

$$\frac{\psi_E}{k_B T} = \left( A_s \sigma_s^2 + A_p \sigma_p^2 + A_{sp} \sigma_s \sigma_p \right) / A_{\text{den}} \qquad \text{(A1)}$$

with $A_s$, $A_p$, $A_{sp}$, and $A_{\text{den}}$ given in Table A1. These coefficients are expressed in terms of three key dimensionless variables: the scaled solute radius $\lambda = r_s/r_p$; the dimensionless pore radius $\tau = \kappa r_p$; and the dimensionless radial position within the pore $\beta = r/r_p$. Note that the parameter $\beta$ does not appear in the expressions using the centerline approximation (Smith and Deen, 1980) since the energy is evaluated at $\beta = 0$.

Bungay and Brenner (1973) developed an analytical expression for the lag coefficient $G(\lambda,0)$ for an uncharged sphere translating in an uncharged cylindrical pore which is valid for all values of the ratio of solute to pore radius ($\lambda$) using matched asymptotic expansions for both small and close fitting spheres. The final result for $\beta = 0$ is given as

$$G(\lambda, 0) = \frac{K_s}{2K_t} \qquad \text{(A2)}$$

The hydrodynamic functions $K_s$ and $K_t$ are expressed as expansions in $\lambda$:

$$\begin{bmatrix} K_t \\ K_s \end{bmatrix} = \frac{9}{4}\pi^2\sqrt{2}\,(1-\lambda)^{-5/2}\left[1 + \sum_{n=1}^{2}\begin{pmatrix} a_n \\ b_n \end{pmatrix}(1-\lambda)^n\right] + \sum_{n=0}^{4}\begin{pmatrix} a_{n+3} \\ b_{n+3} \end{pmatrix}\lambda^n \qquad \text{(A3)}$$

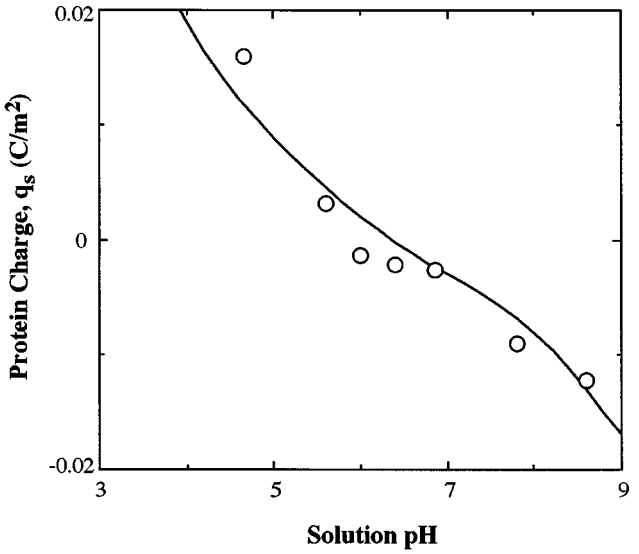


**Figure A1. Surface charge density of ovotransferrin as a function of solution pH.**

Symbols represent literature values from titration data. Solid curve represents model calculation from $pK_a$ values of the charged amino acids, as described in the text.

**Table A1. Coefficients in the Expressions for the Electrostatic Energy of Interaction**

| | Smith and Deen (1980) | Smith and Deen (1983) |
|---|---|---|
| $A_s$ | $\dfrac{4\pi\tau\lambda^4 e^{\tau\lambda} S_0}{1+\tau\lambda}$ | $\left[\dfrac{8\pi\tau\lambda^4 e^{\tau\lambda}}{(1+\tau\lambda)^2}\right]\Lambda$ |
| $A_{sp}$ | $\dfrac{4\pi^2\lambda^2}{I_1(\tau)}$ | $\dfrac{4\pi^2\lambda^2 I_0(\tau\beta)}{(1+\tau\lambda)I_1(\tau)}$ |
| $A_p$ | $\dfrac{\pi^2 h(\tau\lambda)}{\tau^2 I_1^2(\tau)}$ | $\left[\dfrac{\pi I_0(\tau\beta)}{\tau I_1(\tau)}\right]^2\left[\dfrac{(e^{\tau\lambda}+e^{-\tau\lambda})\tau\lambda L(\tau\lambda)}{1+\tau\lambda}\right]$ |
| $A_{\text{den}}$ | $\pi\tau(1+\tau\lambda)e^{-\tau\lambda} - S_0 h(\tau\lambda)$ | $\pi\tau e^{-\tau\lambda} - \dfrac{2(e^{\tau\lambda}-e^{-\tau\lambda})\tau\lambda L(\tau\lambda)\Lambda}{1+\tau\lambda}$ |

$$h(\tau\lambda) = (1+\tau\lambda)e^{-\tau\lambda} - (1-\tau\lambda)e^{\tau\lambda} \qquad L(\tau\lambda) = \coth(\tau\lambda) - 1/\tau\lambda$$

$$S_o = \int_0^\infty \frac{K_1[(\tau^2+\theta^2)^{1/2}]}{I_1[(\tau^2+\theta^2)^{1/2}]}\,d\theta \qquad \Lambda \cong \frac{\pi}{2} I_0(\tau\beta)\sum_{t=0}^{\infty}\frac{\beta^t(2t)!}{2^{3t}(t!)^2} I_t(\tau\beta)\left[\tau K_{t+1}(2\tau) + \frac{3}{4}K_t(2\tau)\right]$$

**Table A2. Expansion Coefficients for Hydrodynamic Functions $K_t$ and $K_s$ in Eq. A3**

| Subscript $n$ | $a_n$ | $b_n$ |
|---|---|---|
| 1 | −73/60 | 7/60 |
| 2 | 77,293/50,400 | −2,227/50,400 |
| 3 | −22.5083 | 4.0180 |
| 4 | −5.6117 | −3.9788 |
| 5 | −0.3363 | −1.9215 |
| 6 | −1.216 | 4.392 |
| 7 | 1.647 | 5.006 |

with coefficients $a_n$ and $b_n$ given in Table A2. Note that the Bungay and Brenner analysis implicitly assumes that electrical effects provide no contribution to the hydrodynamic interactions. This is discussed briefly by Zydney and Pujar (1998).

### *Protein charge*

The net charge on ovotransferrin was calculated from the dissociation of the acidic and basic amino acid residues. The dissociation equilibrium of a typical amino acid residue (for example, an $\alpha$-carboxylic acid) is described by the intrinsic dissociation constant of that ionizable group

$$K^i_{\text{int}} = \frac{[\text{R}-\text{COO}^-][\text{H}^+]}{[\text{R}-\text{COOH}]} \tag{A4}$$

The $H^+$ concentration in Eq. A4 is evaluated at the protein surface and is different than the $H^+$ concentration in the bulk solution due to electrostatic interactions between the charged protein and the charged hydrogen ion. This effect can be described by the Boltzmann distribution:

$$\text{H}^+ = \text{H}^+_b \exp\left(-\frac{e\psi^*_s}{k_B T}\right) \tag{A5}$$

where $H^+_b$ is the bulk $H^+$ concentration, $e$ is the electron charge ($1.609\times10^{-19}$ C), and $\psi^*_s$ is the electrostatic potential at the protein surface. $\psi^*_s$ is linearly related to the protein charge as

$$\psi^*_s = \frac{\epsilon_o \epsilon_r r_s q_s}{(1+\kappa r_s)} \tag{A6}$$

The net protein charge was thus evaluated by simultaneous solution of Eqs. A4 to A6, with Eq. A4 written for all of the ionizable amino acid residues. Additional details on these calculations are provided by Pujar and Zydney (1997). The number and $pK^i_{\text{int}} = -\log(K^i_{\text{int}})$ for the ionizable groups in ovotransferrin are given in Table A3.

**Table A3. Type and Number of Titratable Groups (Williams et al., 1982) on Ovotransferrin**

| Type ($i$) | No. ($n_i$) | $pK^i_{\text{int}}$ |
|---|---|---|
| $\alpha$-Carboxyl | 1 | 2.16 |
| $\beta$-Carboxyl | 46 | 3.90 |
| $\gamma$-Carboxyl | 45 | 4.07 |
| Imidazole | 12 | 6.04 |
| Sulfhydryl | 30 | 8.37 |
| $\alpha$-Amino | 1 | 9.87 |
| $\epsilon$-Amino | 58 | 10.54 |
| Phenolic | 21 | 10.35 |
| Guanidine | 29 | 12.48 |

The model calculations for the surface charge density for ovotransferrin in 10 mM KCl are compared with experimental titration data from Warner and Weber (1953) in Figure A1. The model and data are in good agreement suggesting that the assumption of a uniformly distributed charge over a spherical surface provides a reasonable model for the surface charge characteristics of ovotransferrin.

*Manuscript received Dec. 6, 1999, and revision received Aug. 16, 2000.*